

## Quantum confinement induced strain in quantum dots

Xinyuan Zhang,<sup>1</sup> Pradeep Sharma,<sup>1,2,\*</sup> and H. T. Johnson<sup>3</sup>

<sup>1</sup>*Department of Mechanical Engineering, University of Houston, Houston, Texas 77204, USA*

<sup>2</sup>*Department of Physics, University of Houston, Houston, Texas 77204, USA*

<sup>3</sup>*Department of Mechanical Science and Engineering, University of Illinois at Urbana-Champaign, Urbana, Illinois 61801, USA*

(Received 20 December 2006; published 16 April 2007)

We investigate quantum confinement induced strain in quantum dots. While the impact of mechanical strain on the electronic structure of quantum dots is well studied, the “reverse” effect remains relatively unexplored. Even in the complete absence of external stress, for very small sizes (1–3 nm range), the electronic structure change due to quantum confinement may *induce a strain* in the quantum dot, which in turn will further alter the electronic structure. Despite the limitations of an envelope function approach for small sizes, a multiband analytical model is developed to make explicit the qualitative features of this phenomenon with physical interpretation in terms of acoustic polarons. We quantitatively predict the induced strain due to quantum confinement and the polaron binding energy for the example cases of Si and GaAs. The Si polaron binding energy calculated from the developed model compares favorably with both our density-functional and semiempirical atomistic calculations.

DOI: [10.1103/PhysRevB.75.155319](https://doi.org/10.1103/PhysRevB.75.155319)

PACS number(s): 73.21.La, 73.22.-f

### I. INTRODUCTION

Quantum dots (QDs) promise to be of significant technological importance and, while several barriers remain, are often considered as a basis for various revolutionary nanoelectronic devices and applications ranging from biological labels to quantum computing (see e.g., Refs. 1–3 and references therein). On the scientific side, QDs are a model system to test fundamental quantum-mechanical effects and associated theories. QDs are frequently embedded in or grown on other materials with different elastic constants and lattice parameters. In such a case, due to the lattice mismatch, the consequent elastic strain within the QDs is known to impact their electronic structure and hence optoelectronic properties (see, e.g., Refs. 4–10). Strain can shift the valence and conduction bands, change band gap, cause trapping of carriers and excitons, shift the oscillator strength of indirect-band-gap clusters,<sup>4</sup> and in some piezoelectric materials (e.g., group III-V materials) even cause electrical fields.<sup>5</sup> Although the major effect is due to dilatational strain, axial and shear components can break the cubic symmetry (of most semiconductors) and lead to splitting of the light- and heavy-hole bands. In short, strain mediated control of electronic properties is an intensely researched subject<sup>11–13</sup> of considerable technological importance in the context of both bulk systems and nanostructures. See also a recent review article on this subject.<sup>6</sup>

A wide range of approaches to assess the effect of mechanical strain on band structure is available, ranging from all-electron methods to approximate *ab initio* approaches [self-consistent density-functional theory (DFT)] empirical pseudopotential method, tight-binding method, and envelope function method (EFM). Within each category, there are submethods of varying sophistication. The reader is referred to Refs. 14–21 which provide overviews. For example, EFM, as it is most frequently used, involves taking into account the influence of three valence bands and one conduction band, leading to a set of  $8 \times 8$  Schrödinger-type coupled equations that must be solved numerically for the energy

eigenvalues.<sup>11–14,22</sup> In principle, any number of bands may be included in this approach—the choice of which is dictated by desired accuracy and computational expediency. In this multiband EF model, spin-orbital coupling, light-hole-heavy-hole band mixing, as well as nonparabolicity of carrier dispersion are included. This model has been frequently applied to quantum dots (see, e.g., Refs. 23 and 24). More microscopic approaches which directly involve the electronic degrees of freedom have also been used to investigate strain–electronic-structure coupling for empirical pseudopotential method (see, e.g., Refs. 7, 20, and 21) and (Ref. 25) for tight-binding approach.

In this work we analyze the phenomenon of induced mechanical strain through changes in the quantum confinement (and by extension electronic structure) even in the absence of an externally applied stress. This effect is the converse to the well-studied mechanical strain effect on electronic properties and related to acoustic-type polarons. We modify the standard multiband EFM model to include quantum confinement induced strain and present numerical results for Si and GaAs quantum dots. Band-edge shifts, induced strain field due to quantum confinement, and polaron binding energy are calculated. To verify our model and obtain additional physical insights, we also perform (for smaller size quantum dots) *ab initio* calculations based on parameter-free self-consistent DFT in both local-density and generalized gradient approximations for the polaron binding energy. Larger quantum dots beyond the computational capability of DFT are handled via semiempirical atomistic methods. The conventional EFM, unlike our modified EFM model or atomistic calculations, predicts zero polaron binding energy for all QD sizes.

### II. FORMULATION

In a discrete setting, strain–band-structure coupling (as well as the converse) is related to electron-phonon interaction. The reader is referred to Mahan<sup>26</sup> for a comprehensive review. Electron-phonon interactions can be subdivided into

interactions between electron and optical phonons, electron and piezoelectric phonons, and electron and acoustic phonons. The former two are ignored in the present work.<sup>27</sup> A polaron, in our context, is a charge carrier that carries a localized lattice deformation field with it. Thus, changes in the electronic motion can cause changes in the attached distortion around the charge carrier. For sufficiently small quantum dots, based on this simple physical picture, one may anticipate the possibility of inducing a mechanical strain via changes in the quantum fields. Additionally, if the quantum dot is embedded (or otherwise mechanically constrained), a mechanical stress may also result due to this quantum confinement induced strain.

Based on a discrete model of polarons, an EFM model may be constructed following Emin.<sup>29</sup> Alternatively, in this work, we construct a long-wavelength model in a manner that (if quantum confinement induced strain is ignored) simplifies to the standard multiband  $\mathbf{k} \cdot \mathbf{p}$  approach.

When a carrier (electron or hole) moves in a band, the total energy of the coupled carrier-phonon pair, apart from the unperturbed cohesive energy of the whole system, is the summation of contributions from carrier, elastic field, and the interactions between them.<sup>30</sup> The total Lagrangian in one electron approximation is then

$$L_{tot} = L_{elastic} + L_{electron} + L_{interaction}, \quad (1)$$

where

$$L_{elastic} = \int_V \left[ -\frac{1}{2} \sigma_{ij} \varepsilon_{ij} \right] dV,$$

$$L_{electron} = \int_V \left\{ \frac{i\hbar}{2} [\Psi^\dagger \partial_t \Psi - (\partial_t \Psi^\dagger) \Psi] - \frac{\hbar^2}{2m} \partial_i \Psi^\dagger \partial_i \Psi - \Psi^\dagger V(\mathbf{x}) \Psi \right\} dV,$$

$$L_{interaction} = \int_V \Psi^\dagger(\mathbf{x}, t) (-W_{strain}) \Psi(\mathbf{x}, t) dV(\mathbf{x}). \quad (2)$$

Einstein summation convention is used and the tensor basis is Cartesian.  $\sigma_{ij}$  and  $\varepsilon_{ij}$  are components of the stress and strain tensors, respectively, while  $W_{strain}$  is the deformation potential.  $\Psi(\mathbf{x}, t)$  is the time-dependent wave function. Using standard variational arguments—that is, application of the Euler-Lagrange equations to the functional in Eq. (1)—and separating the time-dependent part [ $\Psi(\mathbf{x}, t) = \psi(\mathbf{x}) e^{-iEt/\hbar}$ ] yields the following governing equations:

$$-\frac{\hbar^2}{2m} \nabla^2 \psi(\mathbf{x}) + V(\mathbf{x}) \psi(\mathbf{x}) + W_{strain} \psi(\mathbf{x}) = E \psi(\mathbf{x}), \quad (3)$$

$$-\frac{\partial}{\partial x_j} \left[ \sigma_{ij} + \psi(\mathbf{x})^\dagger \frac{\partial W_{strain}}{\partial \varepsilon_{ij}} \psi(\mathbf{x}) \right] = 0. \quad (4)$$

Here,  $E$  is the eigenenergy. Equation (3) is the starting point for the derivation of the strain-modified standard multiband EFM model. In Eq. (4), the strain can be decomposed into a part that is induced through the quantum coupling and one

that is present in the uncoupled case  $\varepsilon_{ij}^0$  (i.e., externally applied, or strain resulting from solution of standard elasticity boundary-value problem). Hence, Eq. (4) can be rewritten as

$$\varepsilon_{ij} = \underbrace{\varepsilon_{ij}^0 - S_{ijkl} \psi(\mathbf{x})^\dagger \frac{\partial W_{strain}}{\partial \varepsilon_{kl}} \psi(\mathbf{x})}_{\text{quantum confinement induced strain}}, \quad (5)$$

where  $S_{ijkl}$  is the elastic compliance tensor. Here, the total strain  $\varepsilon_{ij}$  consists of two parts. The bracketed portion is that due to the carrier's quantum field. Usually, the carrier induced strain [i.e., the *quantum confinement induced strain* term in Eq. (4) or (5)] is ignored, thus decoupling elasticity from the quantum fields. Neglecting the bracketed term, while strain can and does impact band structure through the deformation-potential term  $W_{strain}$ , the elasticity equations [Eq. (4)] are solved in an uncoupled approximation suppressing the “reverse” coupling. Retaining this term allows for quantum confinement induced strain and, as can be shown from a discrete viewpoint, polaron states. Even without explicitly specifying the form of deformation potential (which is usually taken to be a linear function of strain), some observations can be made. The extra part that provides a two way coupling in Eqs. (3)–(5) is  $\psi(\mathbf{r})^\dagger (\partial W_{strain} / \partial \varepsilon_{ij}) \psi(\mathbf{r})$ , which inversely scales with the QD volume. A simple order of magnitude calculation involving typical magnitudes of deformation potentials reveals that quantum confinement induced strain coupling is small except for very small quantum dots. This will be made more precise when we present our EFM and *ab initio* results.

Before discussing the more complicated multiband model that describes quantum confinement induced strain, it is useful to consider the simpler effective mass single-band version in which  $W_{strain} = a_d \text{Tr}(\varepsilon_{ij})$  and  $(E_{c/v} - \hbar^2/2m) \nabla^2 + V(\mathbf{r}) = -(\hbar^2/2m^*) \nabla^2$ . Equation (5) then becomes  $\varepsilon_{ij} = \varepsilon_{ij}^0 - (a_d/3K) |\psi(\mathbf{r})|^2 \delta_{ij}$ . Therefore, we obtain a single nonlinear cubic Schrödinger equation for both the conduction and valence bands, given by

$$\left( E_{c/v} - \frac{\hbar^2}{2m^*} \nabla^2 \right) \psi(\mathbf{r}) + a_d \cdot \text{Tr}(\varepsilon_{ij}^0) \psi(\mathbf{r}) - \frac{a_d^2}{K} |\psi(\mathbf{r})|^2 \psi(\mathbf{r}) = E \psi(\mathbf{r}), \quad (6)$$

where  $m^*$  is the effective mass,  $a_d$  is the deformation potential for conduction band or valence band,  $K$  is bulk modulus, and  $E_{c/v}$  is the ground-state band-edge energy of the conduction band or valence band in bulk materials. The quantum confinement induced strain can be obtained by first solving for the wave function through the nonlinear equation (6) and then substituting into Eq. (5). This single-band model neglects the interband interactions and the nonparabolic behavior of energy bands with respect to wave vectors. The single-band model in Eq. (6) is useful for interpreting the numerical multiband and DFT results presented in the next section. The induced strain estimated numerically from Eq. (6) is around 0.024% for a cubic quantum dot of the size around 3 nm (with the choice of  $a_d$  as 6.4 eV and  $K$  as 98 GPa, corresponding to silicon).

To improve on the single-band approach, we expand the wave function in terms of envelope functions,  $\psi(\mathbf{r}) = \sum_{n=1}^{N_b} [\sum_k b_n(\mathbf{k}) e^{i\mathbf{k}\cdot\mathbf{r}}] \phi_{n,\mathbf{k}=0}(\mathbf{r})$ , where  $N_b$  is the number of bands,  $\sum_k b_n(\mathbf{k}) e^{i\mathbf{k}\cdot\mathbf{r}}$  is the envelope function, and  $\phi_{n,\mathbf{k}=0}(\mathbf{r})$  is the atomic basis at  $k=0$ . Then, Eqs. (3) and (5) become (see the Appendix for a detailed derivation)

$$\sum_m [H_{nm}(\mathbf{r}) + W_{nm}(\mathbf{r})] F_m(\mathbf{r}) = E F_n, \quad (7)$$

$$\sigma_{ij} + \sum_{m=1}^{N_b} \sum_{n=1}^{N_b} [F_n^\dagger(\mathbf{x}) D_{ij}^{nm} F_m(\mathbf{x})] = \sigma_{ij}^0, \quad (8)$$

where  $D_{ij} = \partial W_{strain} / \partial \epsilon_{ij}$  is the deformation-potential tensor. We retain only one band for the conduction band due to its  $s$ -type symmetry, while for the valence band a four band scheme<sup>22</sup> is chosen to take care of the large interaction between heavy-hole and light-hole states. More bands may be included, in principle, although the nonlinear nature of the equations makes computation difficult. The resulting deformation-potential matrix is

$$D_{ij}^{mn} = \begin{bmatrix} -a_v \delta_{ij} + q_{ij} & -s_{ij}^* & r_{ij} & 0 \\ -s_{ij} & -a_v \delta_{ij} - q_{ij} & 0 & r_{ij} \\ r_{ij}^* & 0 & -a_v \delta_{ij} - q_{ij} & s_{ij}^* \\ 0 & r_{ij}^* & s_{ij} & -a_v \delta_{ij} + q_{ij} \end{bmatrix}, \quad (9)$$

where the operator matrix is defined as

$$q_{ij} = \begin{bmatrix} -\frac{b}{2} & 0 & 0 \\ 0 & -\frac{b}{2} & 0 \\ 0 & 0 & b \end{bmatrix}, \quad r_{ij} = \begin{bmatrix} \frac{\sqrt{3}b}{2} & -id & 0 \\ -id & -\frac{\sqrt{3}b}{2} & 0 \\ 0 & 0 & 0 \end{bmatrix}, \quad (10)$$

$$s_{ij} = \begin{bmatrix} 0 & 0 & -d \\ 0 & 0 & id \\ -d & id & 0 \end{bmatrix}.$$

### III. MODEL RESULTS, ATOMISTIC CALCULATIONS, AND DISCUSSION

We perform numerical calculations of our nonlinear model on cuboidal Si and GaAs quantum dots. The coupled equations [Eqs. (3) and (5), Eqs. (7) and (8)] are solved by using finite difference method with zero Dirichlet boundary conditions. The resulting large-scale eigenvalue problem is resolved by using the Jacobi-Davidson method.<sup>31</sup> All the required material parameters are obtained from Ref. 32. Our results, shown in Fig. 1, are obtained by solving Eqs. (6)–(8) in a self-consistent iterative manner. To elaborate, the strain components in Eq. (7) are initially set to zero. The solution of the eigenvalue problem in Eq. (7) provides initial estimates of the relative envelope functions  $F_n$  for the ground conduction or valence bands. Equation (8) is then used to obtain modified strains which are inserted into Eq. (7) for further iteration. This self-consistent scheme is carried out until the difference between the successive ground-state band energies is less than 0.1 meV. The difference between the band energy with and without quantum confinement induced

strain is plotted as  $E_{c/v(c)} - E_{c/v(qs)}$ , where the subscripts  $c$  and  $v$  indicate conduction and valence bands, respectively, and  $cl$  and  $qs$  stand for classical and quantum confinement induced strain, respectively.  $E_{c/v(c)} - E_{c/v(qs)}$  is asymptotically equal to  $-(a_d^2/K)|\psi(\mathbf{r})|^2$ . This energy difference is size dependent, and as demonstrated by the simpler single-band model, quadratic in deformation-potential constant. Thus, as evident in Fig. 1, we expect the GaAs QD to have larger quantum confinement induced strain coupling than Si, as the conduction-band deformation potential of GaAs is nearly 1.5 times larger than that of Si. In Fig. 1(b), the silicon QD valence-band energy exhibits a larger shift than GaAs due to its higher valence-band deformation potential. We note that quantum confinement induced strain is negligible for quantum dots with size larger than 2 nm.

The induced strain distributions for conduction and valence bands due to quantum confinement are plotted in Figs. 2(a) and 2(b). The dilation induced by the conduction band is much larger than that by the valence band due to a corresponding difference in their deformation-potential constants. The induced strain field as a function of quantum dot size (and hence quantum confinement) is analyzed in Fig. 3. According to Eq. (4), the strain field is generated even though there is no applied stress. The maximum value of the strain in  $x$ - $y$  plane of the quantum dot is plotted in Fig. 3 for both conduction and valence bands. The spatial distribution of the induced strain is quite nonuniform, and interestingly, for QD sizes larger than 1 nm, the volume average of the dilation induced by the hole polarons is nearly zero. This is explained by noting that the strain contributions from the heavy-hole band and the light-hole band are offsetting.

We now present *ab initio* calculations to verify our model and obtain additional insights. A straightforward way to reconcile the concept of quantum confinement induced strain and/or polarons and validate our modified EFM model is to

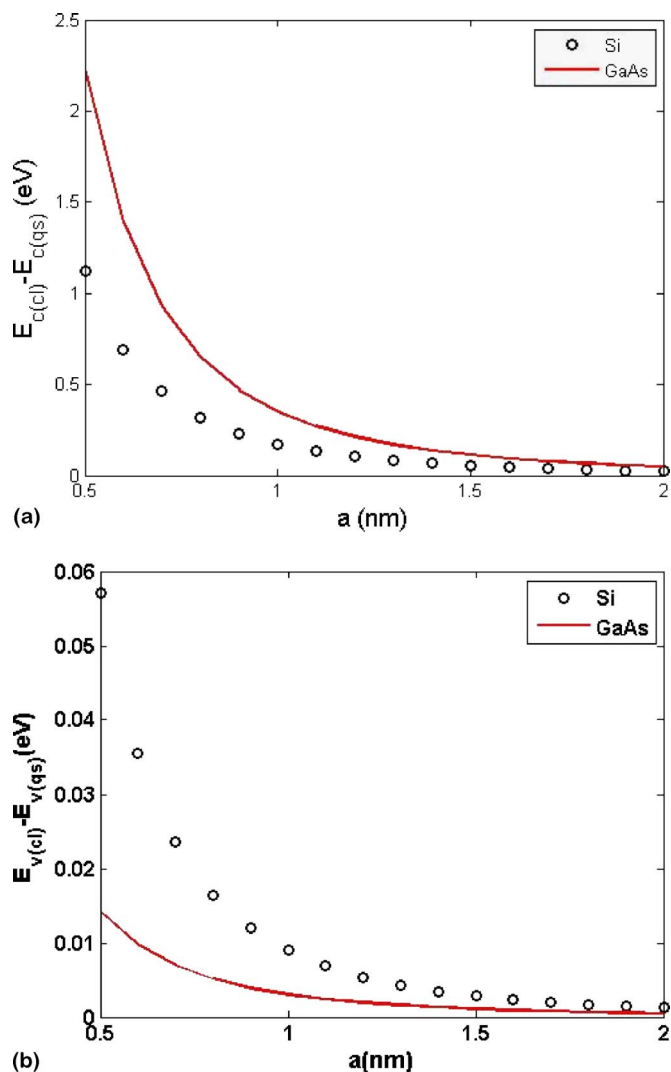


FIG. 1. (Color online) Ground-state band energy shift for (a) the conduction band and (b) the valence band due to quantum confinement induced strain in a cuboidal QD.

contrast the computed electron polaron binding energy with *ab initio* calculations.

The comparison is done solely for Si clusters. The various sized clusters for this study are constructed via truncation of the bulk crystalline Si structure. The dangling surface bonds of the constructed QDs are passivated with hydrogen atoms.<sup>4</sup> The resulting neutral QDs are geometrically optimized with direct inversion iterative subspace method. After appropriate configurational optimization, an electron or hole is doped into the QD and relaxed further from the optimized state of the neutral QD. The change of the total energy from nonrelaxed to relaxed doped quantum dot is the polaron binding energy.<sup>33</sup> For small clusters ( $<1$  nm), the relaxation criterion is set so that the maximum force of the atoms is less than  $0.02$  eV/Å.<sup>4</sup> For larger clusters ( $>1$  nm), the relaxation criterion is chosen as  $0.005$  eV/Å. Both these criteria ensure convergence of the total energy to within  $0.5$  meV. The atomistic calculations are done in two parts: we use parameter-free self-consistent DFT for smaller QDs and a semiempirical method for QDs with more than 500 atoms. The *ab initio*

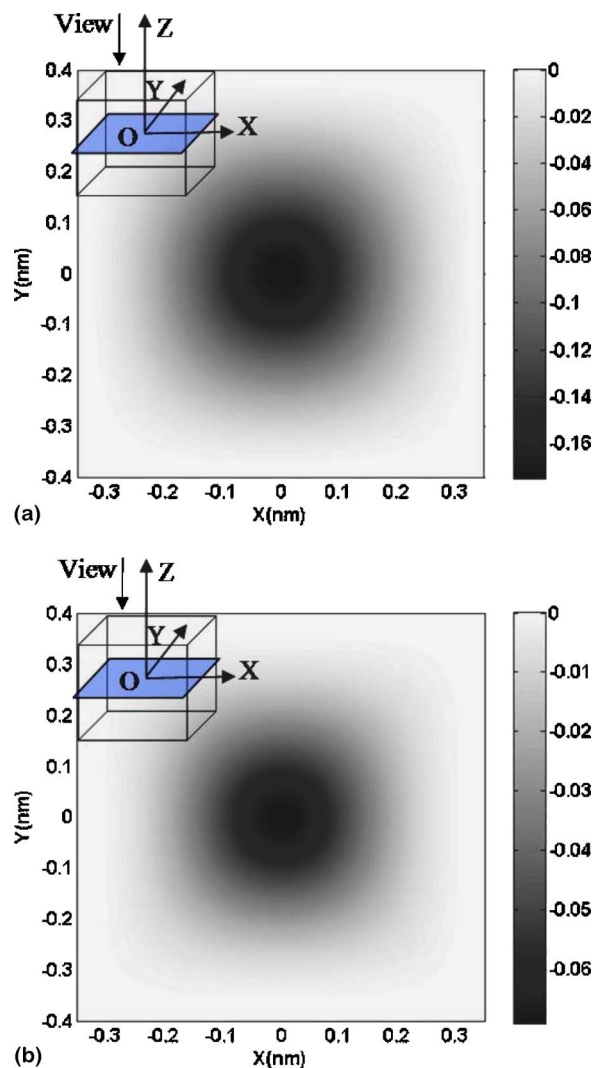


FIG. 2. (Color online) Distribution of strain dilation for cuboidal Si QD ( $a=7$  Å) on the  $z=0$  plane (blue plane, gray in print) viewed from top. (a) Conduction band. (b) Valence band. No external strain is applied and the strain depicted is entirely due to quantum confinement.

calculation is carried out using the  $O(N)$  DFT package OPENMX,<sup>34</sup> with both local-density approximation with Ceperley-Alder functional and generalized gradient approximation (GGA) of Perdew-Burke-Ernzerhof functional without spin-orbital coupling. The semiempirical simulation is performed using PM3 geometric optimization in the GAMESS package.<sup>35</sup> As is well known, DFT is suitable for ground-state total-energy calculations and, for example, underestimates energy gaps. Remedies exist to correct this.<sup>36-39</sup> In any event, detailed calculations examining the accuracy of DFT for strain-electronic-structure coupling were done in Ref. 4, where the supercell DFT results are compared with a more accurate configuration interaction singles calculation as well as an all-electron basis method calculation. Reasonable qualitative and quantitative agreement is found.

In Fig. 4, we compare the polaron binding energy predicted from our modified EFM model, the conventional  $\mathbf{k} \cdot \mathbf{p}$  method (the dotted horizontal line), and our *ab initio* simu-



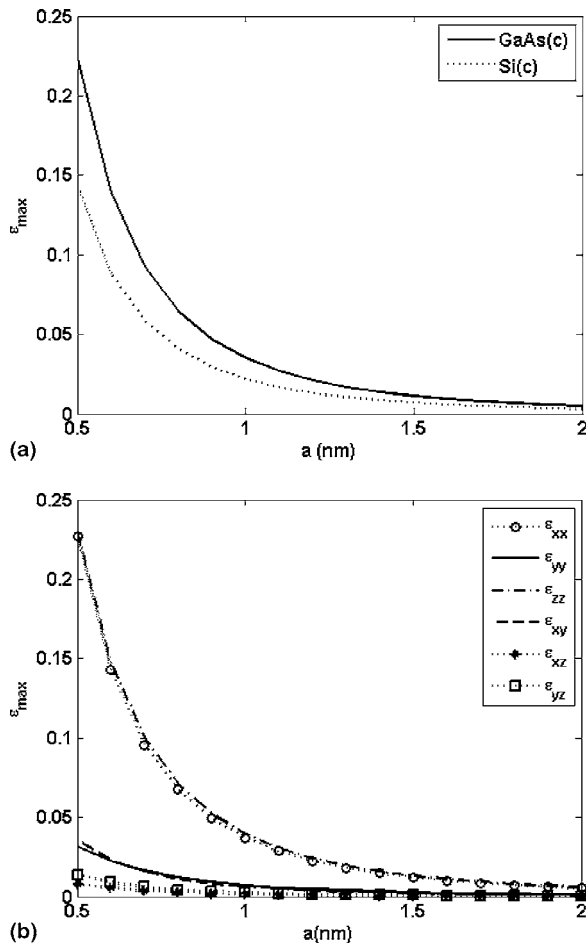


FIG. 3. Variation of the maximum strain with size  $a$  for cuboidal QDs. (a)  $\epsilon_{max} = \max(|\epsilon_{11}|) = \max(|\epsilon_{22}|) = \max(|\epsilon_{33}|)$ . Results for both Si and GaAs are shown. (b)  $\epsilon_{max} = \max(|\epsilon_{ij}|)$ . Only GaAs results are plotted.

lations. As evident, the polaron binding energy from our EFM model [which is identically equal to half of the band energy shift shown in Fig. 1 (Ref. 30)] matches very well with the atomistic results. The conventional EFM approach breaks down for electronic structure calculations around 4 nm or higher. In contrast, the polaron binding energy is in good agreement with atomistic results down to nearly 0.6 nm even though our model is based on an envelope function approach.

For both Figs. 4(a) and 4(b), as expected, the GGA results are better than the LD approximation. As physically intuitive and already expected from the general form of the single-band model, the binding energy increases as the QD size decreases.

While exciton binding energies are not explicitly considered here, they are much larger than the polaron binding energy. The exciton energy for a spherical silicon quantum dot is 3.65 eV (2.30 eV) calculated by using quantum Monte Carlo method for the radius of 25 Å (55 Å).<sup>40</sup> By comparison, the polaron binding energy is 0.15 eV (0.14 eV) at corresponding sizes.

Molecular orbital (MO) or the wave-function plots are shown in Figs. 5(a) and 5(b) for an electron doped QD.<sup>41</sup> The

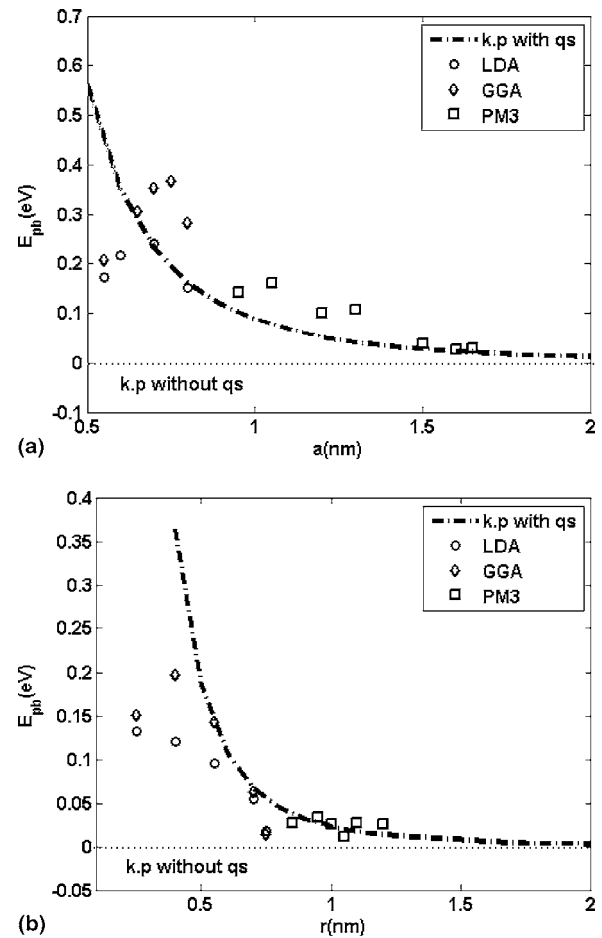


FIG. 4. Comparison of the polaron binding energy calculated from  $\mathbf{k} \cdot \mathbf{p}$  with quantum confinement induced strain (qs in the figure) and from atomistic simulations. (a) Cuboidal Si QD. (b) Spherical QD.

MOs are real value functions in this case since spin-orbital coupling is ignored. In the case of lowest unoccupied molecular orbital (LUMO), an isosurface of 25% of the maximum value of the wave function is plotted, while 50% is chosen to illustrate the highest occupied molecular orbital (HOMO). Red corresponds to positive sign and blue to negative. To illustrate the quantum-mechanical effect of polaron formation, the HOMO-LUMO plots compare the cluster both with and without the inclusion of the effect of polaronic state. The bonding character, which corresponds to increased electron density in the shared regions between Si is, as expected, prominent for HOMO, while the charge density is more localized around the Si atoms in the LUMO plot—consistent with an antibonding character. Comparison of Figs. 5(a) and 5(b) shows that accounting for polaron formation reduces the span of the LUMO isosurface and significantly increases the maximum MO value ( $\sim 100\%$ ). This implies an increase of quantum confinement for the electron. No significant change is seen in the corresponding HOMO plots [Figs. 5(c) and 5(d)]. This feature is also correctly predicted by our modified EFM model that incorporates quantum confinement induced strain (see Fig. 6).

In Fig. 6(a) (which is based on our modified EFM model), we depict the difference of square of the magnitude of par-

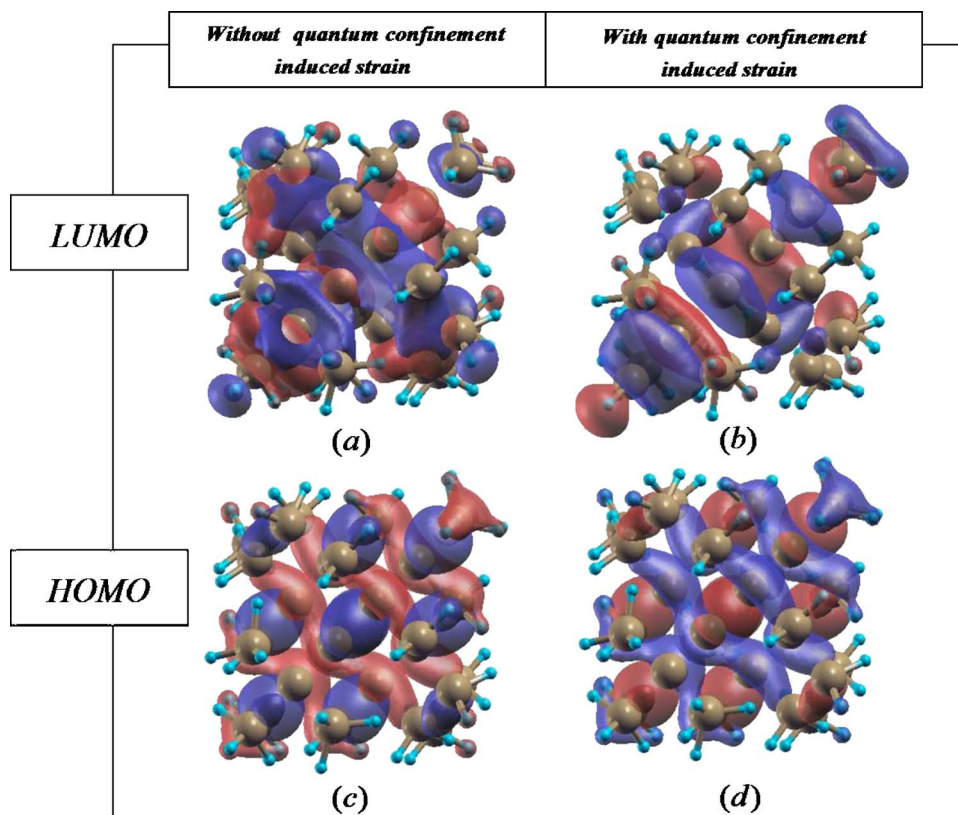


FIG. 5. (Color online) Isosurface plot for the molecular orbitals (wave function) of  $a=7$  Å cuboidal QD, lowest unoccupied molecular orbital (LUMO), and highest occupied molecular orbital (HOMO). Red (lighter gray in print) stands for positive value isosurface and blue (darker gray in print) stands for negative value isosurface. (a) The electron doped LUMO at the value of  $|0.015|$  not incorporating polaron formation. (b) The electron doped LUMO at the value of  $|0.015|$  accounting for polaron formation. (c) The hole doped HOMO at the value of  $|0.02|$  not incorporating polaron formation. (d) The hole doped HOMO at the value of  $|0.02|$  accounting for polaron formation.

title wave function:  $|\psi(\mathbf{r})|_{qs}^2 - |\psi(\mathbf{r})|_{cl}^2$ .  $\psi(\mathbf{r})_{qs}$  incorporates quantum confinement induced strain, while polaronic state is not accounted for in  $\psi(\mathbf{r})_{cl}$ . Consistent with the MO plots shown in Fig. 5, our EFM results indicate increased confinement for the conduction band in the electron doped QD in contrast to negligible qualitative change in the valence band of the hole doped QD. This result is expected based on the analytical form of the single-band model [Eq. (6)]. The polaron binding energy varies as the square of the deformation-potential constant. For bulk silicon, the conduction deformation-potential constant is roughly three times larger than the corresponding valence-band parameter and thus provides justification to the results shown in Figs. 5 and 6.

#### IV. SUMMARY

In summary, we have developed a multiband envelope function approach that incorporates the typically ignored quantum confinement induced strain. This exercise allows us to explicitly interpret this phenomenon in light of all-numerical *ab initio* calculations. Further, due comparison with *ab initio* atomistic calculations reveals that the developed model is capable of capturing the polaron binding energy and can predict induced strain even in the complete absence of external stress provided quantum confinement is appreciable. Future investigation is likely to focus on exploring the role of quantum confinement induced strain (and consequently that of polarons) in the behavior of quantum dots and consequent impact on optoelectronic properties.

#### ACKNOWLEDGMENTS

P.S. and X.Z. acknowledge support of the ONR Young Investigator Program Award No. N000140510662 (Cliff Anderson). We appreciate the discussion with Xihong Peng, Kun Jiao and Taisuke Ozaki regarding the atomistic simulations. The computational facilities were provided by TLC<sup>2</sup> in the University of Houston which is gratefully acknowledged.

#### APPENDIX

The self-consistent polaronic effect in the multiband envelope method can be derived in the following ways. First, the wave function is expanded as

$$\psi(\mathbf{r}) = \sum_{n=1}^{N_b} \left[ \sum_{\mathbf{k}} b_n(\mathbf{k}) e^{i\mathbf{k}\cdot\mathbf{r}} \right] \phi_{n,\mathbf{k}=0}(\mathbf{r}). \quad (\text{A1})$$

Equation (7) may then be obtained following the conventional approach in the multiband  $\mathbf{k}\cdot\mathbf{p}$  method. Here, we focus on the term  $\psi(\mathbf{r})^\dagger \left( \frac{\partial W_{\text{strain}}}{\partial \epsilon_{ij}} \right) \psi(\mathbf{r})$ , which can be written as

$$\psi^\dagger D_{ij} \psi = \langle \alpha | \mathbf{x} | \langle \mathbf{x} | \hat{D}_{ij} | \alpha \rangle, \quad (\text{A2})$$

where  $D_{ij} = \frac{\partial W_{\text{strain}}}{\partial \epsilon_{ij}}$  is a differential operator, while  $\hat{D}_{ij}$  is the corresponding quantum operator. They are related as  $\langle \mathbf{x} | \hat{D}_{ij} | \mathbf{x}' \rangle = D_{ij}(\mathbf{x}') \delta(\mathbf{x} - \mathbf{x}')$ . The wave function is the *position* operating on a specific quantum state, hence,  $\psi(\mathbf{r}) = \langle \mathbf{x} | \alpha \rangle$ .

Equation (A2) may be expanded on position operator  $\mathbf{x}'$  as

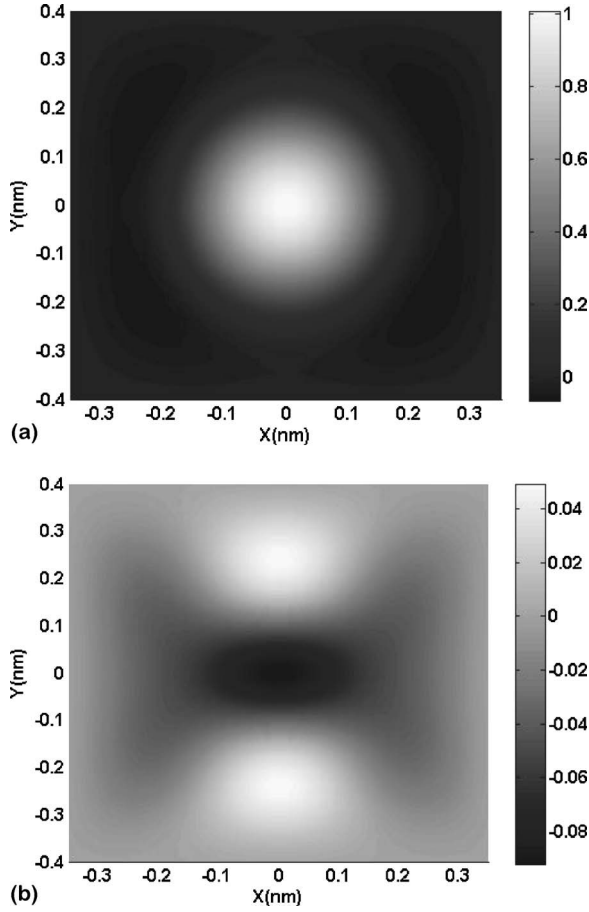


FIG. 6. Results from EFM for  $a=7$  Å cubic QD showing the difference of the square of the magnitude of the wave function,  $|\psi(\mathbf{r})|_{qs}^2 - |\psi(\mathbf{r})|_{cl}^2$ .  $\psi(\mathbf{r})_{qs}$  incorporates quantum confinement induced strain, while polaronic state is not accounted for in  $\psi(\mathbf{r})_{cl}$ . The units are  $\text{nm}^{-3}$ . Part (a) is the electron doped ground-state conduction band, while part (b) is the hole doped ground-state valence band.

$$\psi^\dagger D_{ij} \psi = \int_{\mathbf{x}'} \langle \alpha | \mathbf{x} \rangle \langle \mathbf{x} | \hat{D}_{ij} | \mathbf{x}' \rangle \langle \mathbf{x}' | \alpha \rangle. \quad (\text{A3})$$

Using Eq. (A1), Eq. (A3) can be rewritten as

$$\begin{aligned} \psi^\dagger D_{ij} \psi &= \int_{\mathbf{x}'} \sum_{n=1}^{N_b} \left[ \sum_{\mathbf{k}} b_n(\mathbf{k}) e^{-i\mathbf{k}\cdot\mathbf{x}} \right] \phi_{n,\mathbf{k}=0}^\dagger(\mathbf{x}) \\ &\quad \times \langle \mathbf{x} | \hat{D}_{ij} | \mathbf{x}' \rangle \sum_{m=1}^{N_b} \left[ \sum_{\mathbf{k}'} b_m(\mathbf{k}') e^{i\mathbf{k}'\cdot\mathbf{x}'} \right] \phi_{m,\mathbf{k}=0}(\mathbf{x}'). \end{aligned} \quad (\text{A4})$$

This can be further simplified to

$$\begin{aligned} \psi^\dagger D_{ij} \psi &= \sum_{m=1}^{N_b} \sum_{n=1}^{N_b} \left[ \sum_{\mathbf{k}} b_n(\mathbf{k}) \int_{\mathbf{x}'} [\phi_{n,\mathbf{k}=0}^\dagger(\mathbf{x}) \right. \\ &\quad \left. \times \langle \mathbf{x} | \hat{D}_{ij} | \mathbf{x}' \rangle \phi_{m,\mathbf{k}=0}(\mathbf{x}') e^{i(\mathbf{k}-\mathbf{k}')\cdot\mathbf{x}'}] d\mathbf{x}' \sum_{\mathbf{k}'} b_m(\mathbf{k}') \right], \end{aligned} \quad (\text{A5})$$

while

$$\int_{\mathbf{x}'} [\phi_{n,\mathbf{k}=0}^\dagger(\mathbf{x}) \langle \mathbf{x} | \hat{D}_{ij} | \mathbf{x}' \rangle \phi_{m,\mathbf{k}=0}(\mathbf{x}') e^{i(\mathbf{k}-\mathbf{k}')\cdot\mathbf{x}'}] d\mathbf{x}' = D_{ij}^{nm} \delta_{\mathbf{k},\mathbf{k}'}, \quad (\text{A6})$$

where  $D_{ij}^{nm}$  are the components of  $D_{ij}$  in a Hilbert space consisting of atomic basis  $m$  and  $n$ . Therefore, we can further simplify Eq. (A4) into

$$\begin{aligned} \psi^\dagger D_{ij} \psi &= \sum_{m=1}^{N_b} \sum_{n=1}^{N_b} \left[ \sum_{\mathbf{k}} b_n(\mathbf{k}) D_{ij}^{nm} \delta_{\mathbf{k},\mathbf{k}'} \sum_{\mathbf{k}'} b_m(\mathbf{k}') \right] \\ &= \sum_{m=1}^{N_b} \sum_{n=1}^{N_b} \left[ \sum_{\mathbf{k}} [b_n(\mathbf{k}) D_{ij}^{nm} b_m(\mathbf{k})] \right] \\ &= \sum_{m=1}^{N_b} \sum_{n=1}^{N_b} \left[ \sum_{\mathbf{k}} [b_n(\mathbf{k}) e^{-i\mathbf{k}\cdot\mathbf{x}} D_{ij}^{nm} b_m(\mathbf{k}) e^{i\mathbf{k}\cdot\mathbf{x}}] \right] \\ &= \sum_{m=1}^{N_b} \sum_{n=1}^{N_b} [F_n^\dagger(\mathbf{x}) D_{ij}^{nm} F_m(\mathbf{x})]. \end{aligned} \quad (\text{A7})$$

Equation (A7) may be substituted into Eq. (5) to finally yield Eq. (8).

\*Corresponding author. Electronic address: psharma@uh.edu

<sup>1</sup>P. Alivisatos, Quantum Electronics and Laser Science Conference, 2000 (unpublished), p. 86.

<sup>2</sup>P. Bhattacharya, A. D. Stiff-Roberts, S. Krishna, and S. Kennerly, Int. J. High Speed Electron. Syst. **12**, 969 (2002).

<sup>3</sup>A. Barenco, Contemp. Phys. **37**, 375 (1996).

<sup>4</sup>X. H. Peng, S. Ganti, A. Alizadeh, P. Sharma, S. K. Kumar, and S. K. Nayak, Phys. Rev. B **74**, 035339 (2006).

<sup>5</sup>E. Pan and B. Yang, J. Appl. Phys. **90**, 6190 (2001).

<sup>6</sup>R. Maranganti and P. Sharma, in *Handbook of Theoretical and Computational Nanotechnology*, edited by M. Reith and W. Schommers (Forschungszentrum Karlsruhe, Germany, 2006), Vol. 118.

<sup>7</sup>L. W. Wang, A. J. Williamson, A. Zunger, H. Jiang, and J. Singh, Appl. Phys. Lett. **76**, 339 (2000).

<sup>8</sup>D. A. Faux and G. S. Pearson, Phys. Rev. B **62**, R4798 (2000).

<sup>9</sup>A. D. Andreev, J. R. Downes, D. A. Faux, and E. P. O'Reilly, J. Appl. Phys. **86**, 297 (1999).

<sup>10</sup>C. Pryor, J. Kim, L. W. Wang, A. J. Williamson, and A. Zunger, J. Appl. Phys. **83**, 2548 (1999).

<sup>11</sup>O. Stier, M. Grundmann, and D. Bimberg, Phys. Rev. B **59**, 5688 (1999).

<sup>12</sup>H. T. Johnson, L. B. Freund, C. D. Akyuz, and A. Zaslavsky, J. Appl. Phys. **84**, 3714 (1998).

<sup>13</sup>H. Jiang and J. Singh, Phys. Rev. B **56**, 4696 (1997).

<sup>14</sup>C. Pryor, Phys. Rev. B **57**, 7190 (1998).

- <sup>15</sup>D. Bimberg, M. Grundmann, and N. N. Ledentsov, *Quantum Dot Heterostructures* (Wiley, New York, 1996).
- <sup>16</sup>J. H. Davies, *The Physics of Low-Dimensional Semiconductors: An Introduction* (Cambridge University Press, Cambridge, 2000).
- <sup>17</sup>J. Singh, *Physics of Semiconductors and Their Heterostructures* (McGraw-Hill Higher Education, New York, 1992).
- <sup>18</sup>P. Y. Yu and M. Cardona, *Fundamentals of Semiconductors: Physics and Materials Properties (Advanced Texts in Physics)* (Springer-Verlag, New York, 2004).
- <sup>19</sup>G. Bastard, *Wave Mechanics Applied to Semiconductor Heterostructures* (Wiley, Chichester, 1991).
- <sup>20</sup>L.-W. Wang and A. Zunger, Phys. Rev. B **54**, 11417 (1996).
- <sup>21</sup>A. J. Williamson and A. Zunger, Phys. Rev. B **59**, 15819 (1999).
- <sup>22</sup>E. O. Kane, in *Physics of III-V Compounds, Semiconductors and Semimetals*, Vol. 1, edited by R. K. Williardson and A. C. Beer (Academic, New York, 1966).
- <sup>23</sup>P. C. Sercel and K. J. Vahala, Phys. Rev. B **42**, 3690 (1990).
- <sup>24</sup>Al. L. Efros and M. Rosen, Phys. Rev. B **58**, 7120 (1998).
- <sup>25</sup>J.-Q. Lu, H. T. Johnson, V. D. Dasika, and R. S. Goldman, Appl. Phys. Lett. **88**, 053109 (2006).
- <sup>26</sup>G. D. Mahan, *Many-Particle Physics* (Kluwer Academic, New York/Plenum, 2000).
- <sup>27</sup>The electron–piezoelectric-phonon interaction is important for piezoelectric materials only, and is rarely investigated. The electron–optical-phonon interaction (also called Frohlich polaron or polar coupling), is considerably important for polar or ionic crystals, including many important III-V semiconductor materials, such as GaAs, GaN, CdS, etc. However, as stated in Ref. 28, the electron–acoustic-phonon interaction (investigated in the present work) dominates for reduced dimensional systems, such as QDs. There is no polar coupling between excitons and optical phonons because of the local charge neutrality of excitons in QDs.
- <sup>28</sup>S. Schmitt-Rink, D. A. B. Miller, and D. S. Chemla, Phys. Rev. B **35**, 8113 (1987).
- <sup>29</sup>D. Emin, Phys. Rev. Lett. **28**, 604 (1972).
- <sup>30</sup>D. Emin and T. Holstein, Phys. Rev. Lett. **36**, 323 (1976).
- <sup>31</sup>G. Sleijpen and H. Vorst, SIAM J. Matrix Anal. Appl. **17**, 2 (1996).
- <sup>32</sup>D. J. Paul, Semicond. Sci. Technol. **19**, R75 (2004).
- <sup>33</sup>S. S. Alexandre, E. Artacho, J. M. Soler, and H. Chacham, Phys. Rev. Lett. **91**, 108105 (2003).
- <sup>34</sup>Order N DFT code, OPENMX, available on <http://staff.aist.go.jp/t-ozaki> in the constitution of the GNU GPL.
- <sup>35</sup>The General Atomic and Molecular Electronic Structure System (GAMESS) is available on <http://www.msg.ameslab.gov/GAMESS/> in the constitution of the GNU GPL.
- <sup>36</sup>L. Hedin, Phys. Rev. **139**, A796 (1965).
- <sup>37</sup>A. Zunger, Phys. Status Solidi B **224**, 727 (2001).
- <sup>38</sup>A. Puzder, A. J. Williamson, J. C. Grossman, and G. Galli, J. Am. Chem. Soc. **125**, 2786 (2003).
- <sup>39</sup>E. Degoli, G. Cantele, E. Luppi, R. Magri, D. Ninno, O. Bisi, and S. Ossicini, Phys. Rev. B **69**, 155411 (2004).
- <sup>40</sup>S. Ogut, R. Burdick, Y. Saad, and J. R. Chelikowsky, Phys. Rev. Lett. **90**, 127401 (2003).
- <sup>41</sup>A Crystalline and Molecular Structure Visualization program, XCRYSDEN, is available on <http://www.xcrysden.org> in the constitution of the GNU GPL.